European Rotorcraft Forum

OPEN-LOOP HOVER EXPERIMENT OF A MACH-SCALED SNUF ROTOR FOR ACTIVE VIBRATION CONTROL

Byeonguk Im, goody147@snu.ac.kr, Seoul National University (Korea, Republic of)

Jaeha Ryi, bass83@cnu.ac.kr, Chungnam National University (Korea, Republic of)

Wook Rhee, wookrhee@gmail.com, ICS (Korea, Republic of)

Hyunjae Lee, hyunlee@snu.ac.kr, Seoul National University (Korea, Republic of)

Kunhyuk Kong, drkong123@snu.ac.kr, Seoul National University (Korea, Republic of)

Claire De Poitevin, claire.de-poitevin-de-maureillan@ecole-air.fr, The French Air and Space Force Academy (France)

SangJoon Shin, ssjoon@snu.ac.kr, Seoul National University (Korea, Republic of)

Abstract

Design and open-loop hover experiment of a 4-blade Mach-scaled Seoul National University Flap (SNUF) rotor equipped with an active trailing-edge flap is attempted. Its test is performed on the Seoul National University Rotor Test Stand (SNURTS). First, the rotor hub is improved to withstand the centrifugal loads. In it, the original soft in-plane hingeless rotor hub used for blade optimal design is replaced by a rigid hingeless rotor hub. The multi-body dynamic analysis DYMORE and cross-sectional design tool VABS are used to design the new rotor hub adaptor for the flap blade by utilizing time-marching free-wake analysis. Preliminary hover test using two-bladed OLS teetering hub showed excellent repeatability of the SNURTS, but a torque level of 400N-m should be considered. Rotor test stand modal test response and servo kinematics are fully adjusted into the analysis model. Next, a single active flap blade test is performed to assess the flap driving component. The hysteresis of the flap driving mechanism is identified in a static bench test. Bench dynamic tests of the SNUF blade active flap showed that present flap actuation system has 4/rev bandwidth. In the future, flap deflections will be recorded for the 1-5/rev at 1300 RPM, where the tip Mach number is 0.6. The frequency response of the flap mechanism will be identified under hover centrifugal loads while the blades are still in-track.

1. INTRODUCTION

Recent studies have demonstrated that individual blade control (IBC) using either an active twist rotor (ATR) or an active trailing-edge flaps (ATEFs) can reduce helicopter vibratory loads [1-3]. With the technological advances in the smart material actuator such as piezoelectric actuator, small- and full-scale blades with ATEFs have been designed and tested on whirl towers and in flight [4-9]. In the last few years, the Mach-scaled active flap blade named as SNUF blade was created through comprehensive rotor analysis, computational fluid dynamics analysis, and detailed blade structural analysis [10-13]. The flap driving mechanism was fabricated and tested under expected static centrifugal load for more than two hours with an electromechanical actuator [11]. Fabrication, static and modal testing results of the Seoul National University Flap (SNUF) blade were reported [12]. Further, the identification of the linear HHC flap rotor system and a linear quadratic Gaussian control scheme was investigated [14, 15]. However, such active flap development should include hover stand tests and wind-tunnel tests to verify the design methodologies and control analyses under a rotating test environment. In this paper, hover stand test results of the baseline SNUF rotor blades are presented. Open-loop flap actuation mechanism dynamic characteristics are identified and compared with the static bench tests. Also, a comprehensive rotor analysis based on the rigid hingeless rotor hub are presented.

.

2. EXPERIMENT AND ANALYSIS ON SNUF ROTOR BLADE

2.1. SNUF blade specifications

The previous SNUF blade designed on a soft in-plane hingeless hub has a symmetric NACA0015 airfoil cross-section and a rectangular planform. A 15%c trailing-edge flap was originally located from 65% to 85% span station. Tip Mach number is set

to 0.6, and the radius is 1.5m. Figure 1 shows the cross-sectional configuration and spanwise planform of SNUF blade. Figure 2 shows the previous and present rotor hubs.

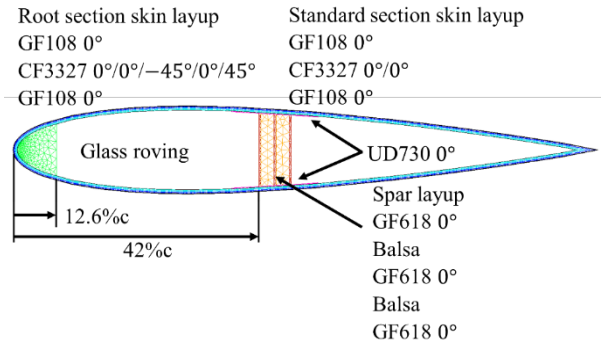

(a) Cross-section of SNUF blade

(b) Planform of SNUF blade

(c) Fabricated blade

Figure 1. SNUF blade configuration

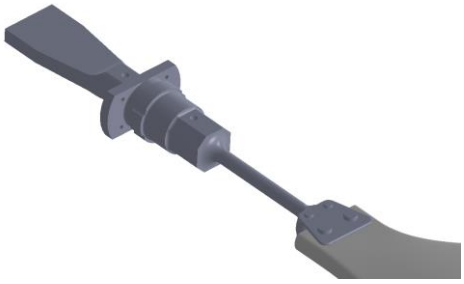

(a) Previous SNUF blade hub

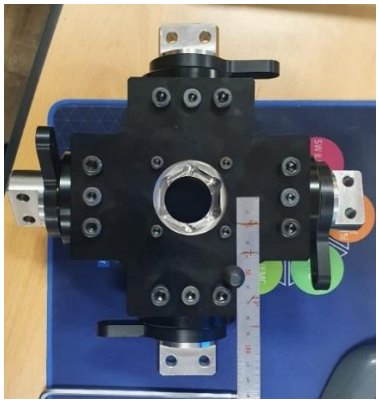

(b) Present SNUF blade hub

Figure 2. Previous and present SNUF hub

2.2. Rotor hub design and analysis

The present SNUF blade hub may have reduced radius of 1.35m because of the modified hub arm length. Therefore, the design of the blade grip connected to the rotor hub may induce a performance change of the active flap rotor system. Since the flap center location and flap length are designed based on the previous rotor hub, the relative flap location will made different unless the hub length is retained. However, the reduced blade radius brings advantages of 1) reduced flap actuator bandwidth, 2) reduced centrifugal load in the blade, and 3) increased adaptability to a wind-tunnel test section.

The variational asymptotic cross-sectional analysis software VABS is used in conjunction with the multi-body dynamics analysis DYMORE. The trailing-edge flap is modeled using several joints in DYMORE as depicted in Fig. 3 (a). Aerodynamic analysis is performed using the unsteady lifting line theory of Peters and the Baghwat-Leishmann time marching free-wake induced inflow analysis as described in Fig. 3 (b). A single trailer wake from the blade tip is assumed. Equations (1-2) shows that the viscous core radius growth model of the vortex filament by Squire is used, and the eddy viscosity parameter a_1 is selected as $a_1 = O(10^{-4})$ following the Mach-scaled rotor experiments [16].

(1) $$r_c(\zeta) = \sqrt{4\alpha\delta\nu\left(\frac{\zeta+\zeta_0}{\Omega}\right)} \equiv \sqrt{r_{c0}^2 + \frac{4\alpha\delta\nu\zeta}{\Omega}}$$

(2) $$\delta = 1 + a_1 Re_v$$

Figure 4 (a) depicts the drawing of the SNURTS 4-blade rigid hingeless hub. Figure 4 (b) shows the discretized cross-sections of the hub and blade using VABS. The hub is designed based on a hingeless structure, and it has an assembly of a thrust bearing and a ball bearing to carry up to 75kN of centrifugal loads.

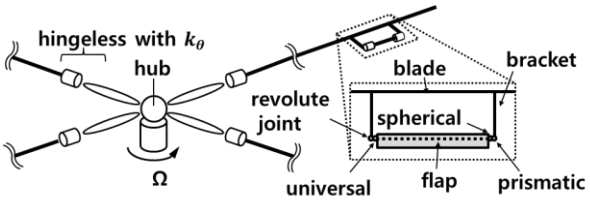

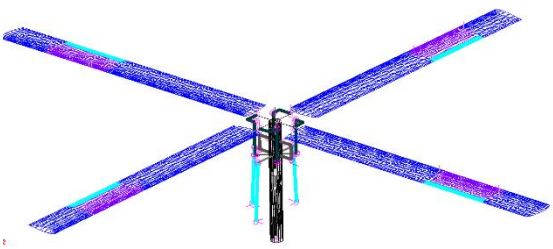

(a) DYMORE representation of the SNUF blade

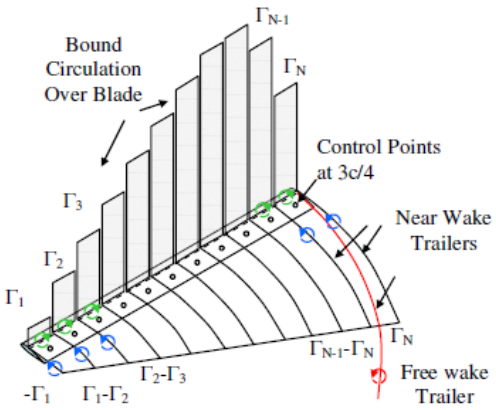

(b) Near wake and far wake trailer [17]

Figure 3. Analysis setup for the SNUF blade

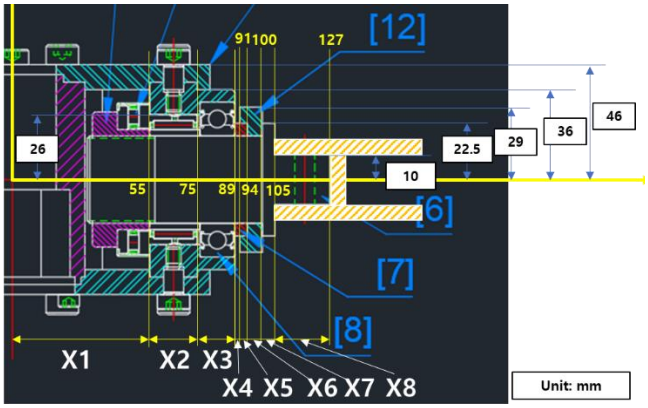

(a) Drawing of the SNURTS rigid 4-blade hub

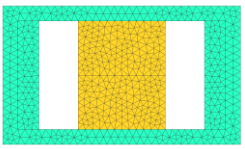

(b) Inboard hub

(c) hub thrust bearing

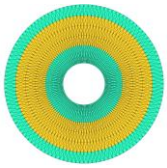

(d) Hub ball bearing

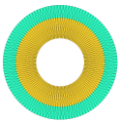

(e) Hub sleeve bearing

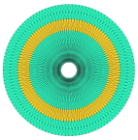

(f) Hub sleeve

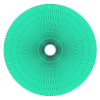

(g) Hub sleeve

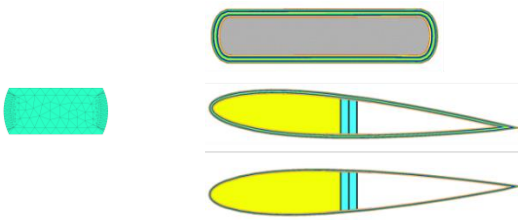

(h) Hub sleeve-fitting to grip

(i) Blade section

Figure 4. Hub drawings and cross-sectional analysis

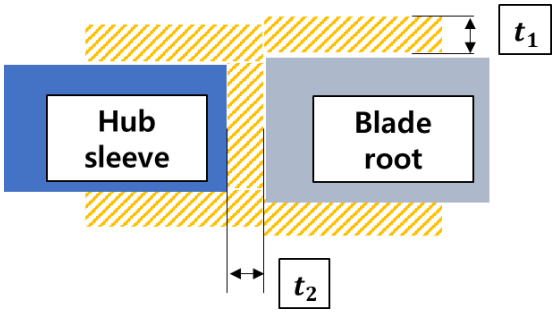

(a) Blade grip design variables

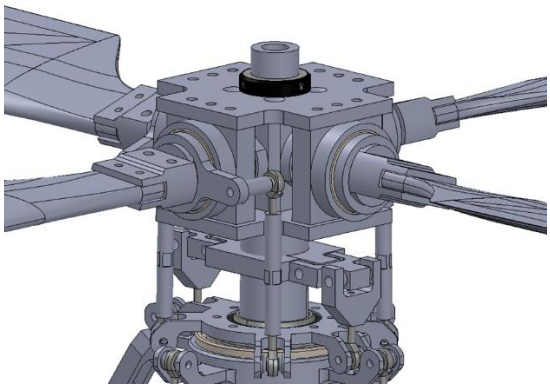

(b) 3-D representation with grip

Figure 5. Blade adaptor design analysis

Figure 5 (a) shows the blade adaptor design variables. A trade-off study is conducted to properly setup the grip thickness t_1 and length t_2. Since the grip length directly affects the rotor radius and overall design specifications, it should be carefully designed. The 2nd flap mode and the 1st torsional mode were examined, which are the two major rotor modes that influences the flap rotor. Also, blade internal stress and strain level were assessed to determine the grip thickness with sufficient safety margins.

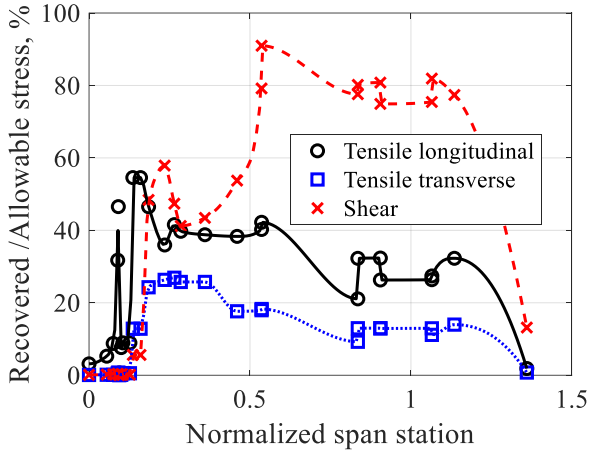

(a) Stress recovery

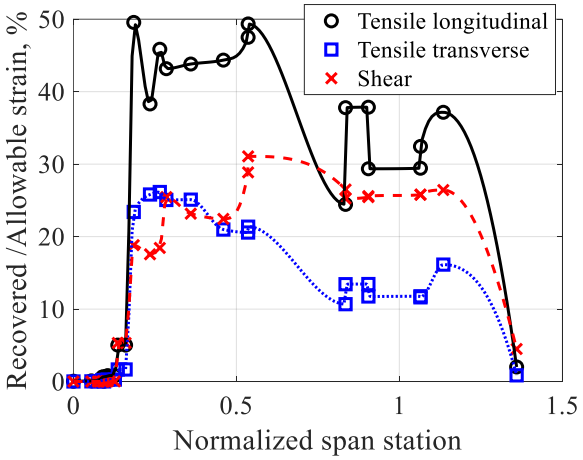

(b) Strain recovery

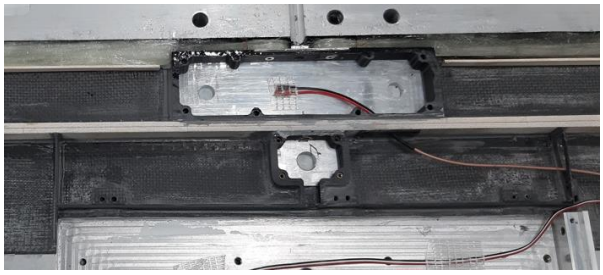

(c) Flap insert part

Figure 7. Structural integrity analysis

Figure 7 (a) and (b) shows the maximum section stress and strain integrity analysis results for adaptor thickness 5 mm. Rotor aerodynamic loads are obtained from hover analysis with $C_T/\sigma = 0.1$. Sectional stress and strain level are recovered using VABS, and a load factor 1.5 is applied. Stress and strain levels increase at the cut-sections for flap insert as the leading-edge glass roving spar is compensated for internal space. Overall stress and strain levels are under the safety limits of each lamina, showing more than average 50% of margin in stress and strain. Further, the stress and strain levels in the rotor hub is relatively low, and there are no significant difference in rotor dynamics and performance with increased grip thickness. Therefore, the grip thickness is set with 5 mm in this study.

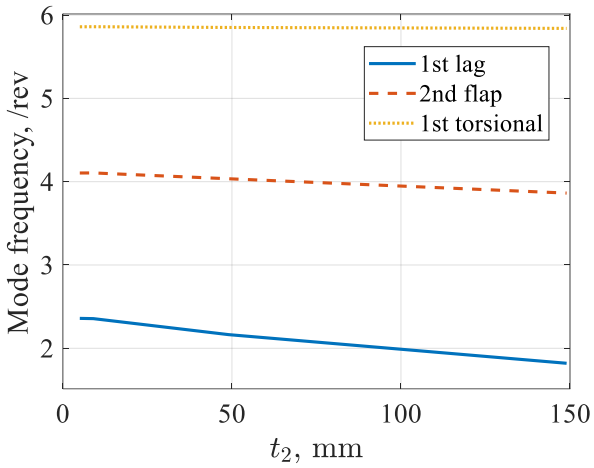

(a) grip length t_2 sweep, $t_1 = 5$mm, pitchlink stiffness = 1×10^8 N/m

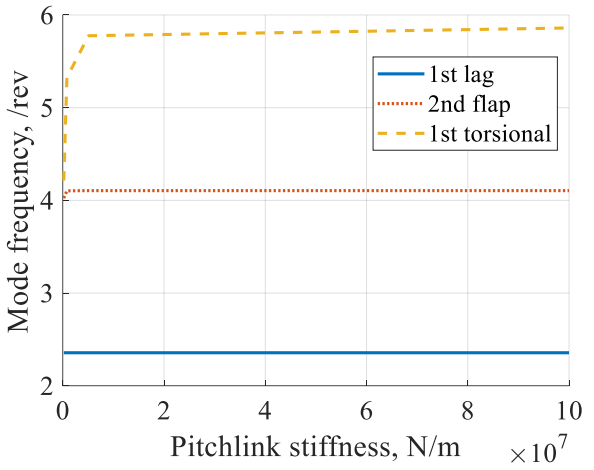

(b) Pitchlink stiffness sweep, $t_2 = 9$mm

Figure 7. Rotor mode frequencies trade study

Figure 7 shows rotor natrual frequencies predicted at nominal 1,300 RPM. Grip length t_2 of 9mm is selected, since it gives the 2nd flap mode placed over 4/rev, which is the blade passing frequency and major flap actuation frequency. The final rotor radius is 1.36m, which is reduced from 1.5m in the previous SNUF blade design.

The blade root composite is expected to be under increased loads as the flexure structures in the previous hub shown in Fig. 2 (a) is removed. Therefore, an additional bolt is added at the blade root to reduce the ply stress level. In Fig. 8, the structural analyses results are presented. The additional bolt reduced root lamina stress about half level.

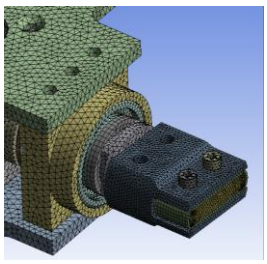

(a) Grip w/ 2-M6 bolt

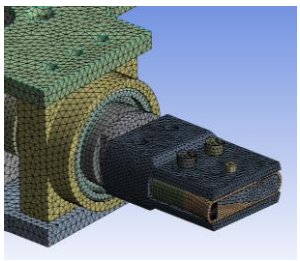

(b) Grip w/ 3-M6 bolt

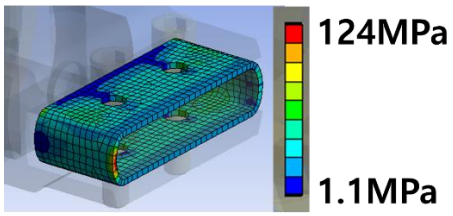

(c) Ply stress, 1st ply w/ 2-M6 bolt

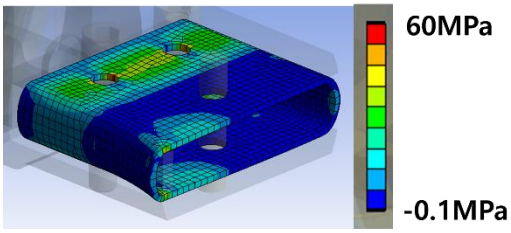

(d) Ply stress, 1st ply w/ 3-M6 bolt

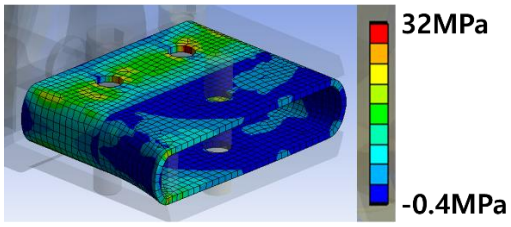

(e) Ply stress, 2nd ply w/ 3-M6 bolt

Figure 8. Additional grip bolt to reduce blade root stress

2.3. SNURTS fundamental analysis

Figure 9 (a) shows the SNURTS setup. It can drive up to 2,000 RPM using an 55kW AC motor. The main shaft is designed to withstand the 1-blade out centrifugal bending moments and shear loads, where the nominal blade centrifugal force is 40kN. A 6-axis fixed balance is mounted, and it is calibrated to measure the loads on the rotor hub center axes. A 20-channel slipring is located inside the bearing tower to tranfer signal between rotating reference frame. Figure 9 (b) shows the console monitoring room which uses NI Labview to manipulate the test signals. Figure 9 (c) shows the test center, which has 12m height and 9m × 9m test space. Test stand can be installed upto 5.5m, and hover out of ground effects height can be achived for rotors with diameters 4.4m.

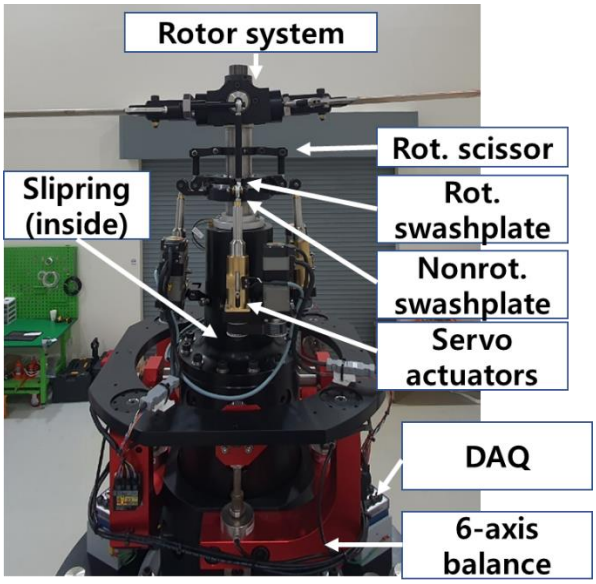

(a) SNURTS main body

(b) SNURTS console monitoring room

(c) Test center

Figure 9. SNURTS setup

To evaluate the rotor test stand integrity and operational standard, hammer modal test and numerical analysis of the test stand is performed. Figure 10 shows the test stand hammer testing. Three accelerometers are installed to measure the modal shape of the motor, pilar, and a main body plate. Figures 11 (a) and (b) show the three-dimensional structural analysis representations. There are at least three elements in the direction of the minimum width of each part. The motor is represented with concentrated mass connected to the motor mount made with MCnylon and main shaft.

Figure 10. Test stand hammer modal test

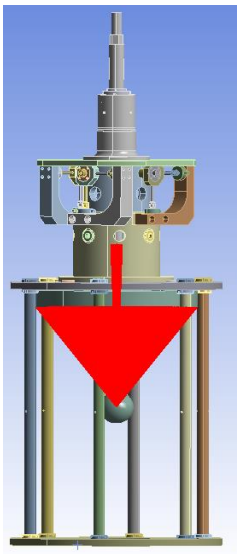

(a) Concentrated motor mass, fixed bottom

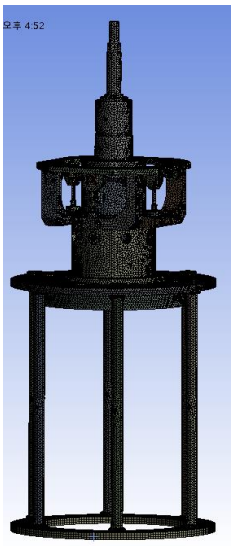

(b) Discretized model

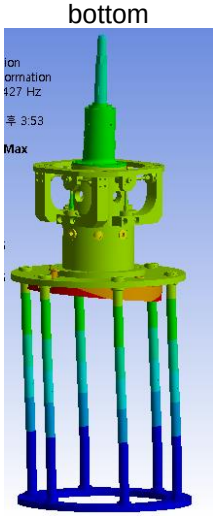

(b) Motor mount and pilar 1st bending 4.8 Hz

(c) Motor mount and pilar 2nd bending 15.1 Hz

(d) Pilar torsion 22 Hz

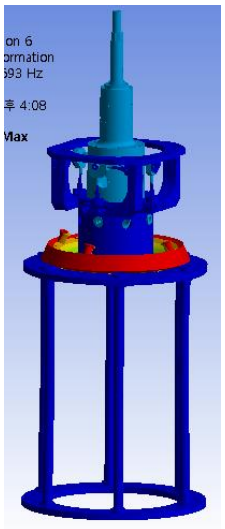

(e) Motor mount coning mode 22.1 Hz

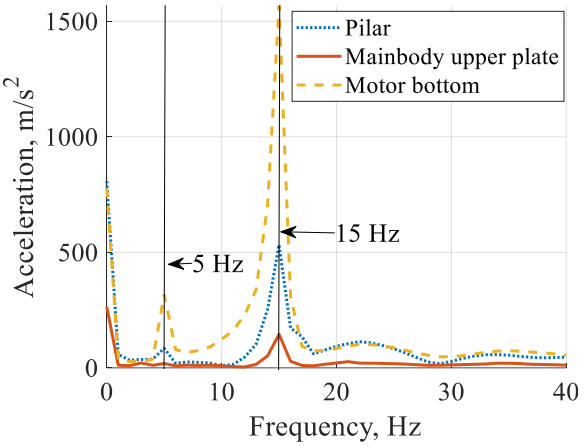

(f) Modal test result of the main body

Figure 11. Structural modal analysis of the SNURTS

Figure 12 (c) ~ (e) show predicted modal response of the test stand main body. Figure 11 (f) shows measured accelerometer response from the hammer test. Contact stiffness among the lock nuts and pillars are adjusted to match the measured frequencies. As it is predicted by the analysis, the motor mount and pilar 2nd bending mode shows most significant magnitude of modal vectors. Also, the motor mount bending mode is realized by the measurement from the motor bottom side. As a result, operational RPM should avoid the two bending modes 300 RPM and 900 RPM. Also, this is consistent with the 2500N thrust class balance and 55kW motor test capabilities, where Mach scaled blades with RPM over 1100 is mainly installed.

2.4. Preliminery 2-blade OLS rotor test

2.4.1. Test overview and analysis setup

To evaluate the SNURTS, a preliminary hover test is performed. A 2-bladed teetering hub with OLS blades is tested and compared with the reference test result [17, 18]. Table 1 shows the specification of the OLS blade.

Table 1. Specifications of the OLS blade [17]

Radius, *R*	3.437 ft
Length (blade only)	2.968 ft
Chord	4 inch
Airfoil	NACA 0012
Twist	None
Root Attachment	Teetering hub
Solidity	0.06192
Precone	1.2°
Under Sling	0.03 ft
Rotation	CCW
Pitch-flap coupling	0°
Nominal speed	1120 RPM

Figure 12 shows DYMORE representation of the OLS 2-blade teetering hub. Main shaft is modeled from the bearing tower end. Figure 13 plots the discretized cross-sections of the hub and the blade using VABS.

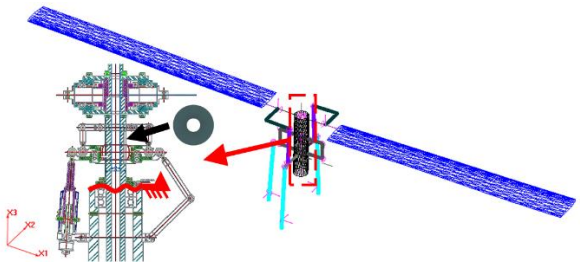

Figure. 12 DYMORE configuration of the OLS rotor system

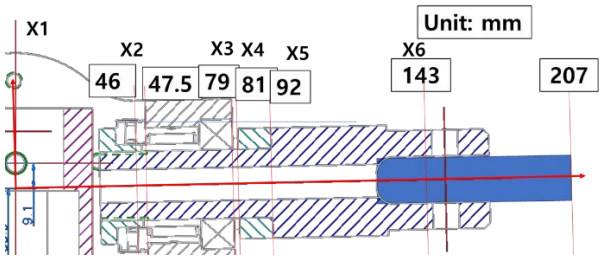

(a) Rotor hub drawing

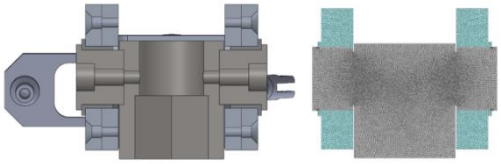

(b) X1 segment cross-section

(c) X2 segment cross-section

(d) X3 segment cross-section

(e) X4 segment cross-section

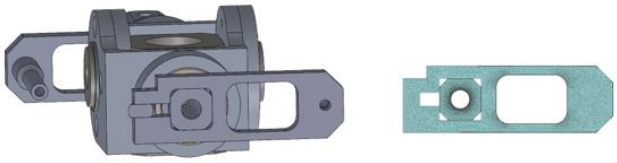

(f) X5 segment cross-section

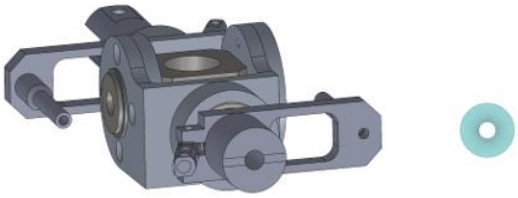

(g) X6 segment cross-section

Figure 13. Teetering hub cross-sectional analysis

Stiffness and damping of the teeter hinge are identified by measured accelerations. Figure 14 shows the experimental setup for the rotor nonrotating natural frequencies.

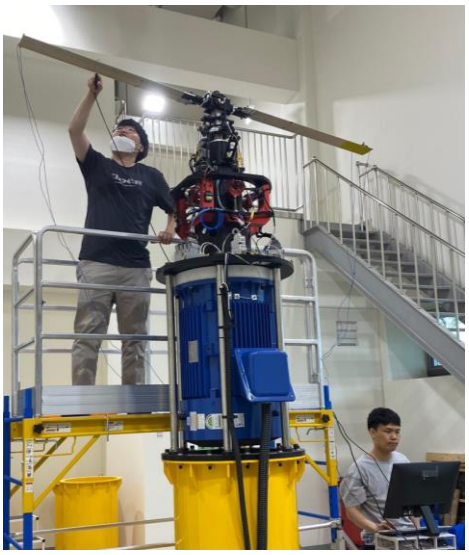

(a) Rotor impact test

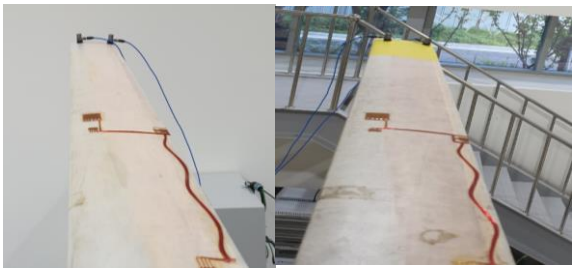

(b) Accelerometers attached at each blade tip

Figure 14. Set-up for the rotor nonrotating natural frequencies test

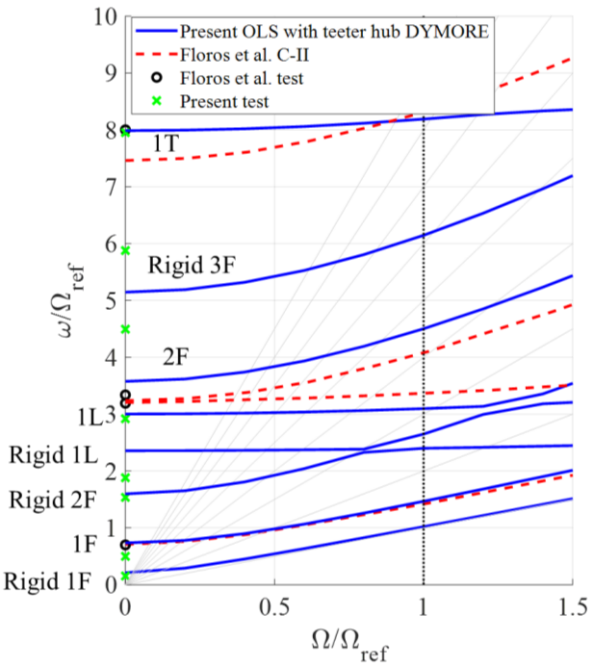

(a) with present OLS test data

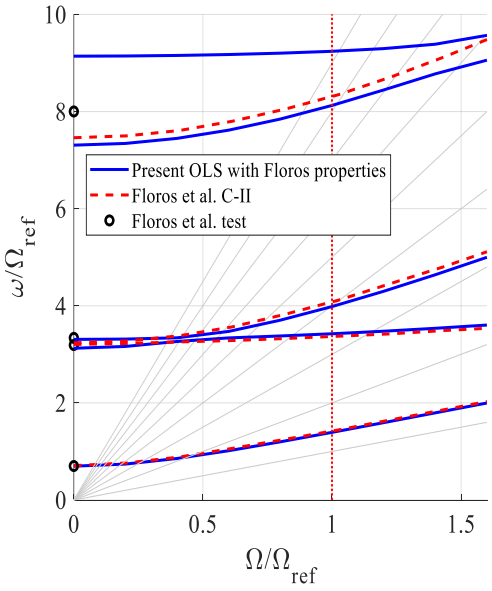

(b) with reference properties [17]

Figure 15. Fanplot

Figure 15 shows the fanplot with identified nonrotating frequencies of the present OLS teetering hub and the reference result. The present hub has relatively lower teeter hinge stiffness, so the lower flap and lag modes are identified.

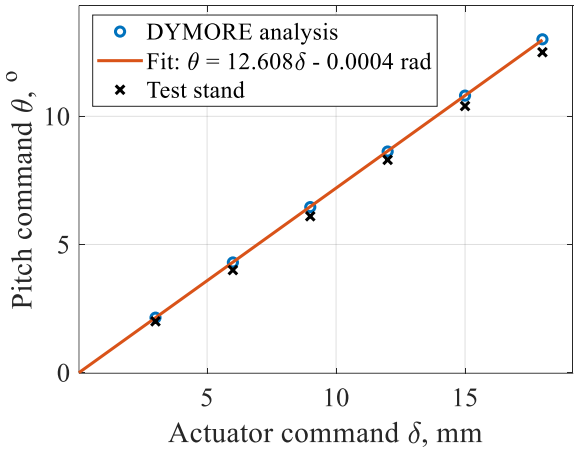

Figure 16. Pitch calibration result

Figure 16 shows the measured test stand collective pitch angle to the servo actuator command and analysis simulation results. The present DYMORE analysis slightly overpredicts the pitch action where the discrepancy in the slope is about 8%.

2.4.2. Hover test results and correlation

Collective pitch sweep test is conducted in nominal RPM. Thrust and torque are measured for each collective pitch angle 2,4,6,8,10 and 12°. Three sets of the test were performed with all the doors closed, and an extra open-door test was performed to see the door effects. The test stand showed excellent repeatability in the closed-door test. The open-door test resulted in decreased thrust and torque, where additional inflows decreased sectional effective angle of attack.

Figure 17 shows the results of the test and analysis. In this test, OLS test on KARI GSRTS in 2012 is regarded as the reference, because the same blades were used. Also, the figure of merit of NACA0012 untwisted planform can never achieve such high levels of figure of merit as described in Fig. 17 (c). Fig. 17 (b) shows that torque discrepancy is up to -9Nm. The main cause of the discrepancy is due to the balance capacity, where it is designed to measure 400Nm class SNUF rotor system. Since the OLS rotor system has at most 40 N-m torque, the relative resolution is quite as small as 1/10.

In Fig. 17, the black lines indicate DYMORE prediction. CAMRAD-II analysis is also performed to compare between the comprehensive codes. Both codes with the uniform inflow options predict nearly identical thrust, but DYMORE underpredicts torque. Further, the free wake analysis of DYMORE even under predicts torque, while the thrust levels are adjusted by the viscosity parameters. Therefore, SNURTS should use blades with moderate torque levels within 400 Nm.

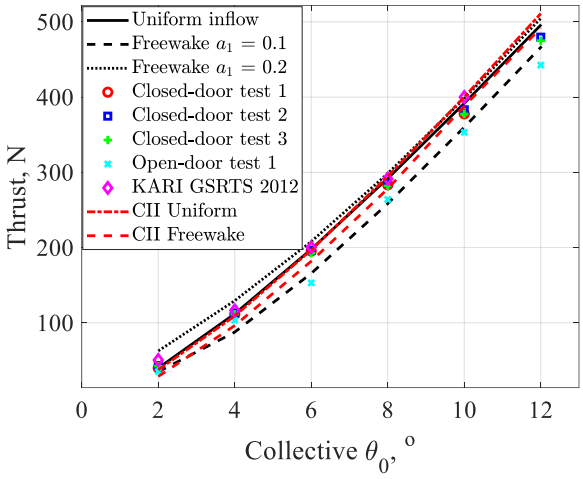

(a) Thrust vs. collective

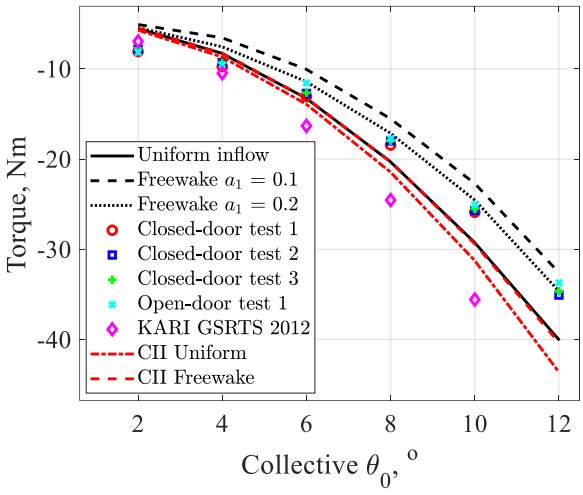

(b) Torque vs. collective

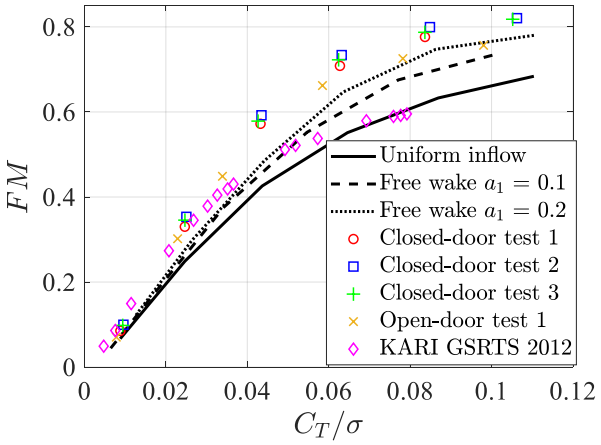

(c) Figure of merit (FM)

Figure 17. Hover test and analysis result of the OLS rotor

2.5. Testing of the active flap blade

2.5.1. Dynamic characteristics measurement of the flap mechanism in bench

Prior to hover test, a bench test for the active flap is conducted to check the dynamics and possible non-linearities. Piezoelectric actuators generally have hysteresis nonlinear characteristics. On the other hand, hysteresis depends on the frequency where it imposes a large phase distortion on low frequencies and relatively small phase distortion on high frequencies [19, 20].

Figure 18 shows the bench test setup for the active flap system equipped within the blade. Compared with the previous tests performed on a fixed table, the actuation system is structurally coupled with the blade. In this paper, the flap driving voltage is described in the DAQ output level, not the amplified level which has a static gain of 20.

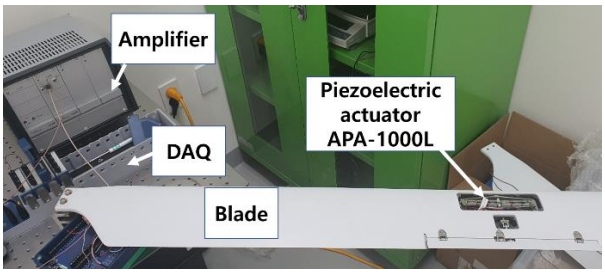

Figure 18. Bench test setup for the SNUF blade

An analog hollow potentiometer 3382G-103 is installed to measure the active flap deflection, and it is calibrated by a digital protractor. Figure 19 shows the calibration results.

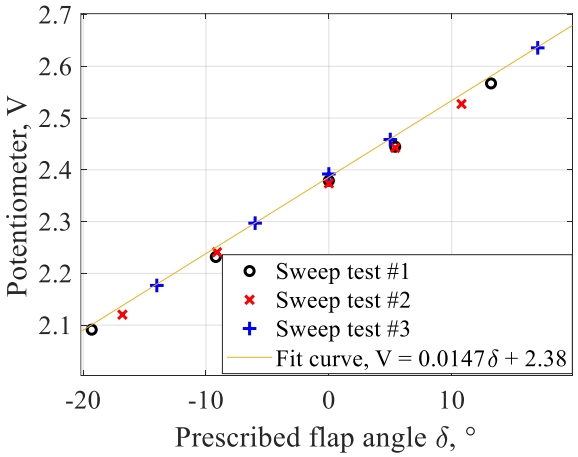

Figure 19. Active flap potentiometer calibration

The active flap system also has free play where it can be linearized by software. Equation (3) describes input linearization using 1st order input mapping where V_{cmd}^* is the mapped input from V_{cmd}, V_{th} is threshold freeplay input voltage, and V_{sat} is the input saturation. Small amount of the dead zone V_{dead} is required to remove unnecessary actions near the zero input. Figure 19 depicts measured the free play and linearized results. Excessive free play is compensated and the response is linearized so that it can be fit into a linear curve.

$$V_{cmd}^* = \frac{V_{sat}-V_{th}}{V_{sat}-V_{dead}}(V_{cmd} - V_{dead}) + V_{th} \quad (3)$$

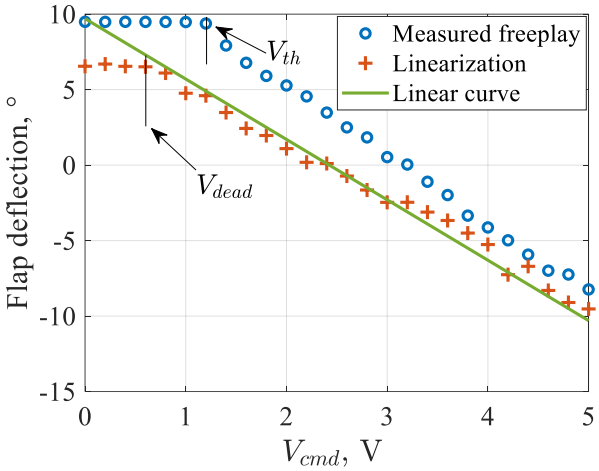

Figure 20. Active flap linearization

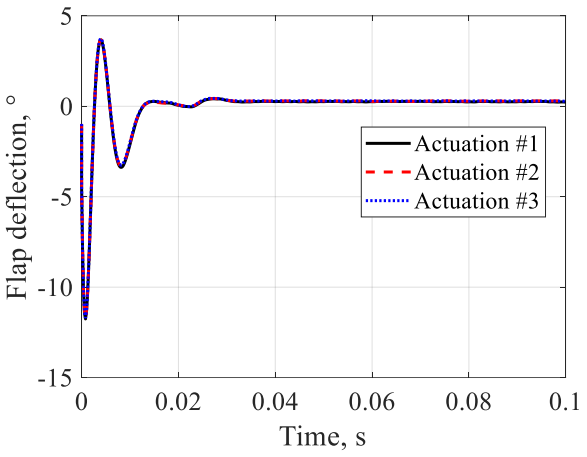

(a) 2V step input

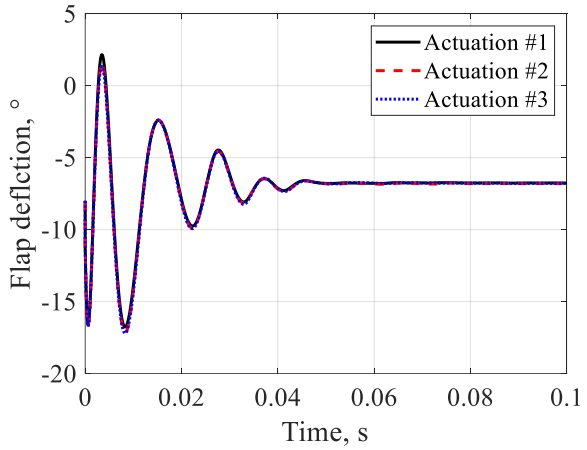

(b) 3V step input

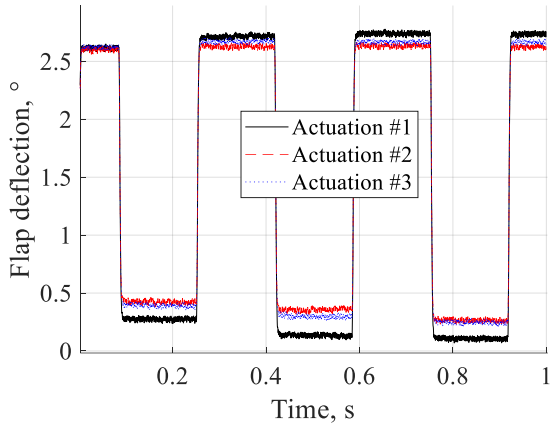

(c) 2V square wave input

Figure 21. Transient responses of present active flap in bench test

Figure 21 shows the transient responses of the present flap mechanism that has hysteresis. As shown in Figs. 20 (a) and (b), a one-way response can be repeated, but in Fig. 21 (c), the pulses invoke hysteresis where each actuation show differences in the peak-to-peak level. Also, Figs. 21 (a) and (b) show that flap dynamics is affected by the amount of the input. Figure 22 shows identified transfer functions from step responses of Figs. 21 (a) and (b). Both have the similar phase responses, but the magnitude has different characteristics. Therefore, the flap actuation input should be limited to ensure a linear response, while this should be tested either in a rotating environment.

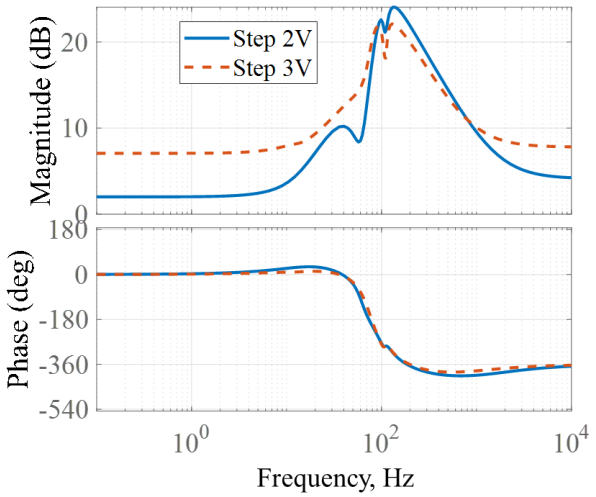

Figure 22. Identified transfer functions from different step input amplitude

In the bench test, a 2V peak-to-peak input is adequate for producing $\pm 4°$ active flap deflection. Also, it is preferable to use the smaller input and output signals to drive the system as a linear state. Therefore, a transfer function is estimated using the 2V square wave responses.

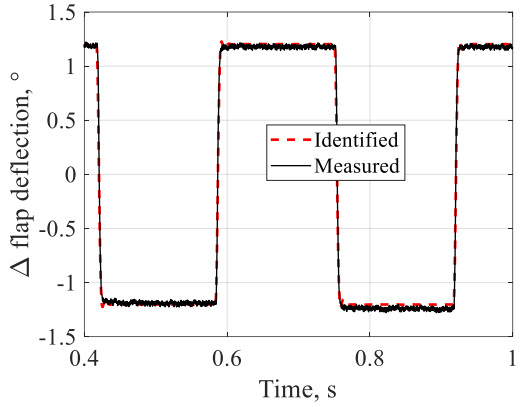

(a) Transfer function identification in time-domain

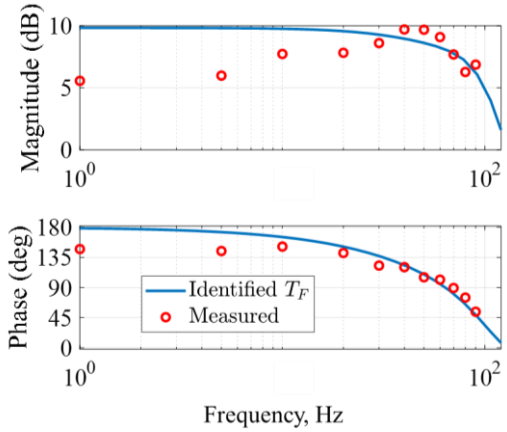

(b) Frequency response

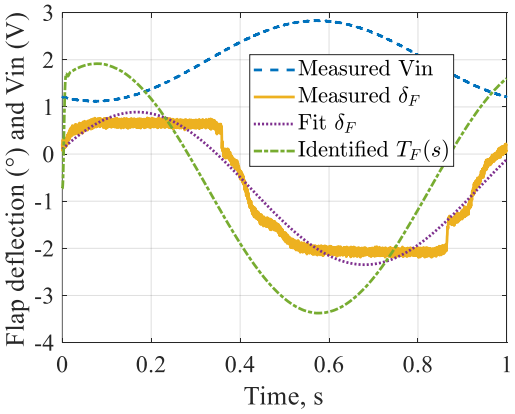

(c) 1 Hz

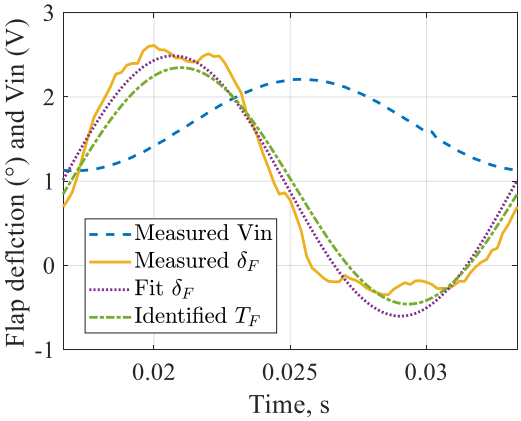

(d) 60 Hz

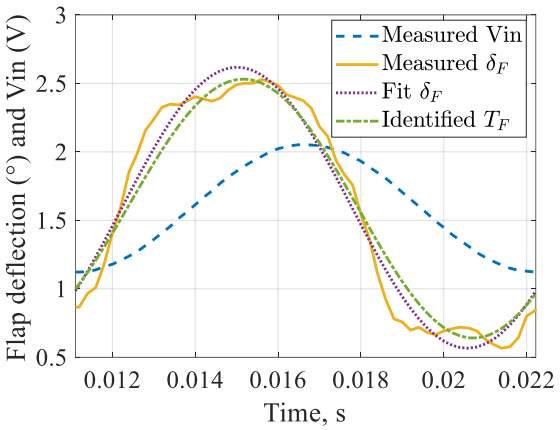

(e) 90 Hz

Figure 23. Transfer function identification in bench

Figure 23 (a) shows the identified transfer function in time domain which has no zeros and 3 poles as shown in Eq. (4)

(4) $$T_F(s) = \frac{-4.82\times10^8}{s^3+966s^2+634700s+1.56\times10^8}$$

Figure 23 (b) shows frequency response of the transfer function and measured responses from each frequency. The phase is well matched from 10 Hz. Lower frequencies have steady phase delays due to high hysteresis effect and frictions, whereas high frequency signal can be regarded as linear. The bandwidth of the present active flap in bench is 90 Hz, which is 4.2/rev. Actuation above the cutoff frequency can damage the system.
Figures 23 (c) ~ (e) show the harmonic responses of the active flap. It is noteworthy that in the lower frequencies up to 20 Hz, the flap deflection is saturated and cannot be recovered as a full sinusoidal response due to excessive frictions. Therefore, as shown in Fig 23. (b), the actual response amplitude will be larger if the flap actuation is not saturated.

2.5.2. Modal test results of the blades

Figure 24 shows the free-free modal frequencies obtained from NASTRAN analysis and the test. Blade 1 is the first fabricated blade, and it has a 20% low torsional frequency. Blade 2-4 were produced at the same period, and finally Blade 5 is fabricated to have a 4-blade set with matched torsional frequency.

Mode shape vectors are produced by quadrature picking for modal displacement. If the k-th mode shape vector is denoted as $\boldsymbol{\phi_k} = [\phi_{1k}, \phi_{2k}, \cdots, \phi_{nk}]^T$, $k = 1 \cdots n$, it will be approximately proportional to $\mathrm{Imag}[H_i(j\omega)]_{\omega=\omega_k}$ where $H_i(j\omega)$ is the i-th column of $H(j\omega)$, $i = 1 \cdots n$.

(5) $$MAC_{ij} = |\psi_i^T \phi_j|^2 / [(\phi_j^T \phi_j)(\psi_i^T \psi_i)]$$

where ψ or ϕ are designated as eigenvector from

the test or analysis. Figure 24 shows the obtained MAC values. MAC value is larger than 0.9 for the first three modes. Since the experiment reveals the coupled flap bending and torsion mode while the analysis has the uncoupled 2nd torsional mode, MAC value for those modes becomes smaller than 0.9.

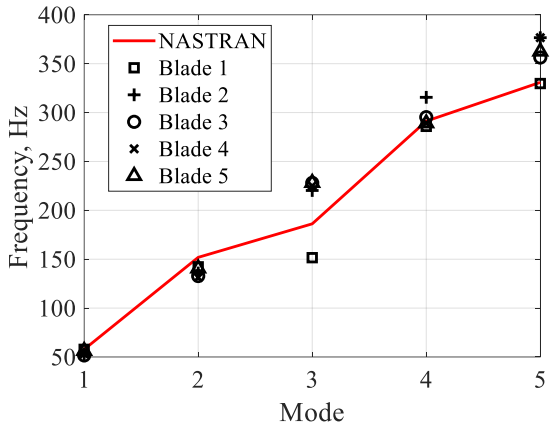

(a) Natural frequencies obtained from NASTRAN and experiment

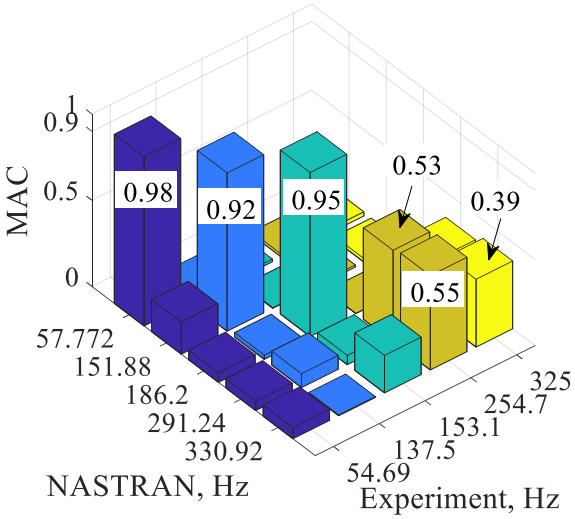

(b) Present MAC plot

Figure 24. Blade modal test results

2.5.3. Open-loop hover test simulation

Based on the preliminary tests and analysis, open-loop SNUF hover test and analysis is to be scheduled. Due to some technical discussions, the open-loop SNUF blade test will be conducted after this paper submission. The baseline SNUF rotor collective sweep test and RPM sweep test will correct the analysis options with correlations. Then, a hover efficiency variation test with prescribed trailing-edge flap deflection can be performed.

Figure 25 shows predicted figure of merit for SNUF rotor on SNURTS.

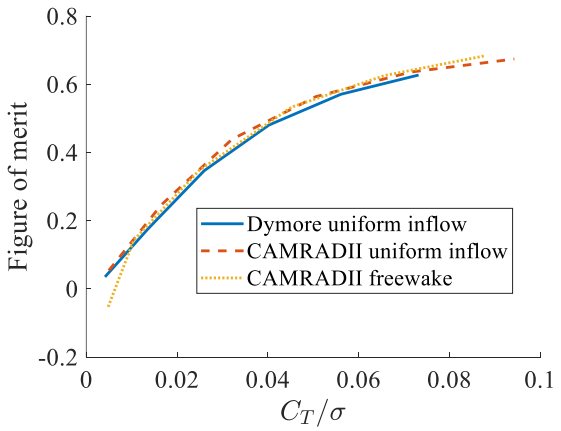

Figure 25. Figure of merit prediction of SNUF baseline rotor

3. CONCLUSION AND FUTURE WORKS

In this paper, the recent developments of SNURTS for the testing of SNUF blade equipped with a trailing-edge flap and relevant analysis results are presented. New hub grip design parameters are explored. Next, the test stand modal test are performed and correlated with three-dimensional structural analysis. Preliminary hover test using two-bladed OLS teetering hub showed the repeatability of the SNURTS, but a balance resolution should be considered. Bench dynamic tests of the SNUF blade active flap showed that present flap actuation system has 4/rev bandwidth. However, actual closed-loop bandwidth should be set much below from the actuator bandwidth to obtain a proper performance.
In the future, system identification procedure on the hover stand and wind-tunnel will be implemented. It will be examined if any substantial improvements are required in the blade design or flap mechanism design. Also, a variable twist control for the vibratory loads will be studied.

4. REFERENCES

[1] Ham, N. D., “Helicopter Individual Blade Control and Its Applications,” American Helicopter Society 38th Annual Forum Proceedings, St. Louis, MO, 1983.

[2] Shin, S. J., Cesnik, C. E. S., and Hall, S. R., “Closed-Loop Control Test of NASA/ARMY/MIT Active Twist Rotor for Vibration Reduction,” Journal of the American Helicopter Society, Vol. 50, (2), 2005, pp. 178–194. doi: 10.4050/1.3092854

[3] Friedmann, P. P., “On-Blade Control of Rotor Vibration, Noise, and Performance: Just Around the Corner? The 33rd Alexander

Nikolsky Honorary Lecture," American Helicopter Society 69th Annual Forum, Phoenix, AZ, May 2013. doi: 10.4050/JAHS.59.041001

[4] Koratkar, N. A., and Chopra, I., "Open-Loop Hover Testing of a Smart Rotor Model," AIAA Journal, Vol. 40, (2), August 2002, pp. 1495–1502. doi: 10.2514/2.1834

[5] Koratkar,N.A., and Chopra, I., "Wind Tunnel Testing of a Smart Rotor Model with Trailing Edge Flaps," Journal of the American Helicopter Society, Vol. 47, (4), October 2002, pp. 263–272. doi: 10.4050/JAHS.47.263

[6] Roget, B., and Chopra, I., "Closed-Loop Test of a Rotor with Individually Controlled Trailing-Edge Flaps for Vibration Reduction," Journal of the American Helicopter Society, Vol. 55, (1), 2010, pp. 1-10. doi: 10.4050/JAHS.55.012009

[7] Straub, F. K., Anand, V. R., Birchette, T. S., and Lau, B. H., "SMART Rotor Development and Wind Tunnel Test," 35th European Rotorcraft Forum, Hamburg, Germany, Sept. 2009.

[8] Roth, D., Enekl, B., and Dieterich, O., "Active Rotor Control by Flaps for Vibration Reduction - Full Scale Demonstrator and First Flight Test Results," Proceedings of 32nd European Rotorcraft Forum, Maastricht, The Netherlands, September 12–14, 2006.

[9] Padthe, A. K., Friedmann, P. P., and Prasad, J. V. R., "High-Fidelity Linear Time-Invariant Models for Higher Harmonic Closed-Loop Rotor Control Studies," Journal of the American Helicopter Society, Vol. 62, (012003), 2017, pp. 1-15, doi: 10.4050/JAHS.62.012003

[10] Eun, W. J., Sim, J. S., Lee, S. W., and Shin, S. J., "Advancement of the SNUF Blade Design through Flap Configuration Parametric Study and Optimization Framework," AHS International 73rd Annual Forum & Technology Display, Fort Worth, Texas, May 9-11, 2017.

[11] Eun, W. J., Im, B. U., and Shin, S. J., "Endurance Test of the Revised SNUF blade with Active Trailing-Edge Flap," The 6th Asian/Australian Rotorcraft Forum / Heli Japan, Kanazawa, Japan, November, 2017.

[12] Visconti, U., Eun, W. J., Sim, J. S., Lee, S. W., and Shin, S. J., "Design Improvements and Flap Deflection Evaluations with Considering Centrifugal Load on Active Trailing Edge Flap," Aircraft Engineering and Aerospace Technology, 2017.

[13] Eun, W. J., Sim, J. S., Lee, S. W. and Shin, S. J., "Further Improvements in the SNUF Blade Design by Numerical Design Optimization Framework," ASCE's Journal of Aerospace Engineering, 2018.

[14] Im, B. U., Lee, C. B., Eun, W. J., and Shin, S. J., "System Identification of SNUF Blade Equipped with an Active Trailing-Edge Flap," The 7th Asian/Australian Rotorcraft Forum, Jeju Island, Korea, October, 2018.

[15] Im, B., Lee, C., Kee, Y., and Shin, S.J., "Investigation of Linear Higher Harmonic Control Algorithm for Rotorcraft Vibration Reduction", Journal of Dynamic Systems Measurement and Control, Vol. 143, (1), 2021, pp. 011008-1 - 011008-12. doi: 10.1115/1.4048369

[16] Bhagwat, M. J., and Leishman, J. G., "Generalized Viscous Vortex Model For Application To Free-Vortex Wake And Aeroacoustic Calculations," 58th American Helicopter Society Annual Forum and Technology Display, Montreal, Canada, June 2002.

[17] Floros, M. W., Gold, N. P., and Johnson. W., "An Exploratory Aerodynamic Limits Test with Analytical Correlation", American Helicopter Society 4th Decennial Specialists' Conference, Jan 2004.

[18] Kim. S.H., et al, "Study on the Technology for Green Quiet Rotor", KARI, Basic Technology Research Society, 2012.

[19] Roget, B., "Simulation of Active Twist and Active Flap Control on a Model-Scale Helicopter Rotor," 24th Applied Aerodynamics Conference, June 2006, San Francisco, CA.

[20] Lee, T., and Chopra, I., "Design of piezostack-driven trailing-edge flap actuator for helicopter rotors," Smart Materials and Structures, Vol. 10, (1), May. 2000, pp. 15–24.

[21] Zhu, W., and Rui, X. T., "Hysteresis modeling and displacement control of piezoelectric actuators with the frequency-dependent behavior using a generalized Bouc-Wen model," Precision Engineering, Vol. 43, (31), Jan. 2016, pp. 299–307.